Platinum Monolayer Electrocatalysts

Jia X. Wang (Primary Contact), Kotaro Sasaki, and Miomir Vukmirovic
Brookhaven National Laboratory
Upton, NY 11973-5000
Phone: 631-344-2515
Email: jia@bnl.gov

DOE Manager: Nancy Garland
Phone: 202-586-5673
Email: Nancy.Garland@ee.doe.gov

Project Start Date: July 1, 2015
Project End Date: September 30, 2019

Overall Objectives

- Synthesizing high performance electrocatalysts for the oxygen reduction reaction (ORR) consisting of about one monolayer (ML) Pt shell on cores made of stable, inexpensive metal, metal alloy, nitride, phosphide, or carbide nanoparticle cores.
- Increasing activity and stability of Pt ML core-shell catalysts and stability of carbon supports while reducing noble metal contents.

Fiscal Year (FY) 2019 Objectives

- Synthesize PtNiN nanocatalysts on various carbon supports for possible benefits in controlling particle size, improving mass transport, and enhancing support durability.
- Study lattice phase behavior of PtNiN nanoparticles to guide effort in further enhancing ORR activity and catalyst durability.
- Identify key structural parameters for quality control in scale-up synthesis.
- Deliver selected PtNiN catalysts on commonly used carbon and on corrosion-resistant graphene for membrane electrode assembly (MEA) tests.
- Validate PtNiN as highly active and durable ORR catalysts for meeting/exceeding the DOE targets listed in Table 1.

Technical Barriers

This project addresses the following technical barriers from the Fuel Cells section of the Fuel Cell Technologies Office Multi-Year Research, Development, and Demonstration Plan[1]:

- (A) Durability
- (B) Cost
- (C) Performance.

Technical Targets

This project aims at optimizing the core-shell component distribution and crystalline structure of PtNiN catalysts for meeting/exceeding the DOE 2020 targets listed in Table 1. The performance of intermetallic $L1_0$-PtCo catalyst reported in 2019 is included as the state-of-the-art catalyst for comparison. Two PtNiN catalysts supported on commonly used carbons were tested for cell performance and catalyst durability by Jacob Spendelow at Las Alamos National Laboratory (LANL) and Jian Xie's group at Indiana University Purdue University Indianapolis (IUPUI). Another two samples were created using IUPUI-made functional graphene (f-G and f-nanoG) as the supports and tested for support durability.

The DOE technical targets and our current project status are listed in Table 1 for comparison.

FY 2019 Accomplishments

- Enhanced activity and durability of PtNiN on Ketjenblack EC 300J (KB) by promoting formation of intermetallic-like PtNiN nanoparticles, which exhibited comparable activity and catalyst durability as that of intermetallic $L1_0$-PtCo catalyst in MEA tests.
- Gained a better understanding of the effect of chemical ordering on lattice strains and structural stability, which helps in identifying key structural parameters for synthesis optimization.
- Optimized synthesis procedure and parameters for producing high crystalline nanoparticles

[1] https://www.energy.gov/eere/fuelcells/downloads/fuel-cell-technologies-office-multi-year-research-development-and-22

with Pt monolayer on chemically-ordered Pt_2Ni_2N cores.

- Synthesized Pt_{ML}-Pt_2Ni_2N crystalline nanoparticles on functional graphene using seeded growth method at sufficiently low temperature for retaining functional groups, which enables combination of highly active and durable PtNiN with corrosion-resistant graphene for meeting durability targets for both catalyst and support concurrently.

Table 1. MEA Performance of PtNiN Catalysts Compared to DOE Targets and the State-of-the-Art $L1_0$-PtCo Catalyst (fc161_spendelow_2019_o presentation at 2019 AMR)

Characteristic	Units	Target	$L1_0$-PtCo	Pt_{ML}-Pt_2Ni_2N			
Measured at			LANL		IUPUI		
Carbon support[a]			VC	KB	VC	f-G	f-nanoG
Pt mass activity (MA)[b] @ 0.9V	A mg^{-1}	>0.44	0.60	0.49	0.20	0.19	0.30
MA loss after catalyst AST [1]	%	<40%	40%	35%	-5%		
MA loss after support AST [2]	%	<40%				38%	36%
Power density at 0.67 V, H_2/air	W cm^{-2}	>1	0.89	0.81	0.41	0.28	0.47
Voltage at 0.8 A cm^{-2}	mV		743	725	644	535	612
Voltage loss at 0.8 A cm^{-2} [1]	mV	<30	26	34	25		
Voltage loss at 0.8 A cm^{-2} [2]	mV	<30				169	117
Pt loading	mg cm^{-2}	<0.125	0.106	0.121	0.08	0.090	0.10
Pt weight percent on carbon	wt %		20%	21%	24%	26%	37%

[a] VC – Vulcan XC72, KB – Ketjenblack EC 300J, f-G and f-nanoG – functional (nano-)graphene
[b] Pt mass activities and their loss after accelerated stress test (AST) for catalyst or support were measured with H_2/O_2. All others were measured with H_2/air, 150 kPa(abs).
[1] after 30,000 cycles of 0.6 V (3s) – 0.95 V (3s) for catalyst durability.
[2] after 5,000 cycles of 1–1.5 V at 500 mV s^{-1} for support durability.

INTRODUCTION

Various conductive materials including nitrides, phosphides, and oxides are options for developing advanced electrocatalysts. PtNi nitride is selected for developing ORR catalysts because Ni is a very good activity promotor for ORR, but prone to dissolution under polymer electrolyte membrane fuel cell operation conditions, and nitriding can stabilize Ni. One apparent advantage of nitriding is that the PtNiN samples made by reducing Pt and Ni precursors in ammonia gas flow can be used as is without acid treatment for removing Ni in the surface region. This is attributed to the formation of a Pt monolayer skin on a Ni-enriched bimetallic nitride core during nitriding. Questions remain on whether facet/shape control or high crystallinity or increasing N content can further improve PtNiN nanocatalysts. In this period, progress was made in better understanding the lattice structure of the bimetallic nitride core and in synthesizing highly crystalline nanocatalysts on various carbon supports. We thank Jacob Spendelow at LANL and Jian Xie at IUPUI for their efforts in carrying out MEA tests for our PtNiN samples. Validating PtNiN as a highly active and durable ORR catalyst in MEA is a major goal of this project.

APPROACH

In catalyst synthesis, three approaches were found effective in improving the activity and durability of PtNiN nanocatalysts. The first is annealing PtNiN nanoparticles at 560°C for 9–18 hours with ammonia gas. KB was found as a better support than Vulcan XC 72 (VC) for minimizing growth of particle size. The sample tested in MEA at LANL has an average particle size of 4.7 nm determined by transmission electron microscopy. The second approach pursues high uniformity and narrow particle size distribution for fine tuning Ni content to promote formation of Pt monolayer on chemically-ordered Pt_2Ni_2N and Pt_1Ni_3N cores. A Pt_{ML}-Pt_2Ni_2N sample on VC support was tested at IUPUI. The third synthesis method uses preexisting Pt nanoparticles as the seed to catalyze Ni reduction at a low temperature for making PtNiN nanoparticles with high Ni content and narrower size distribution. This method was used for synthesizing the MEA-tested PtNiN/f-g and PtNiN/f-nanoG samples because it significantly improved particle size control and retaining functional group on graphene.

RESULTS

A PtNiN/KB sample made by high temperature annealing was tested at LANL. With H_2/O_2 feed, the Pt mass activity is 0.49 A mg^{-1} and a loss after catalyst accelerated stress test (AST) is 35%, exceeding the DOE targets. In H_2/air, the power density reached 0.81 W cm^{-2} at 0.67 V and a loss in voltage at 0.8 A cm^{-2} is 34 mV (Figure 1a). While improvements are needed to meet the targets of 1 W cm^{-2} power density and <30 mV voltage loss, the results validate PtNiN as an active and durable ORR catalyst comparable to $L1_0$ PtCo catalysts (Table 1).

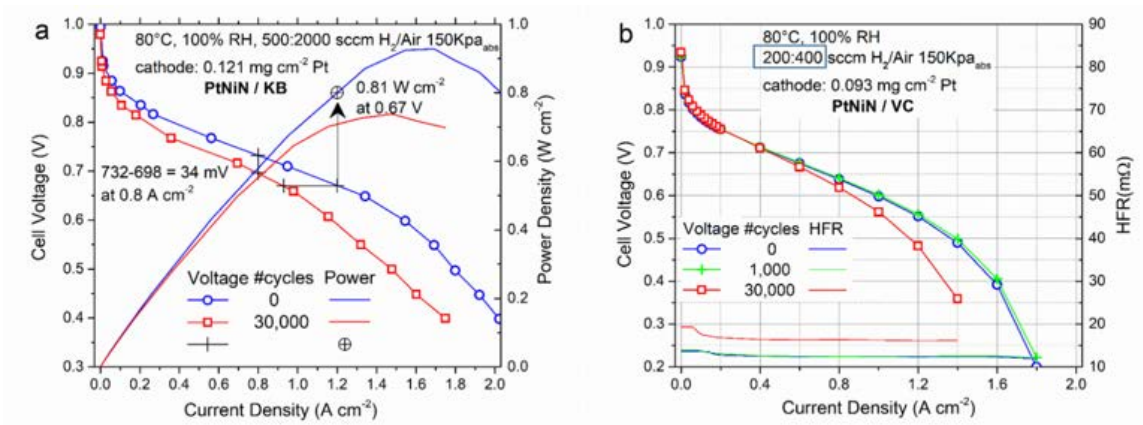

Figure 1. MEA polarization curves before and after catalyst AST for (a) PtNiN/KB measured at LANL and (b) PtNiN/VC measured at IUPUI

The PtNiN/VC sample tested at IUPUI was made by the second approach of fine-tuning synthesis parameters to promote formation of Pt monolayer on crystalline Pt_2Ni_2N particles. The result showed catalyst durability exceeding the targets with no loss of Pt mass activity at 0.9 V and 25 mV voltage loss at 0.8 A cm^{-2} (Figure 1b). However, the power density and Pt mass activity are much lower than the PtNiN/KB sample tested at LANL. The likely causes include (1) lower catalyst loading (0.093 vs. 0.121 mg cm^{-2} Pt) lowers power density, and (2) poorer mass transport due to lower flow rates (200:400 sccm H_2/air vs. the common 500:2000 sccm) and different hardware parts in the test cells.

We also tested some PtNiN samples under support AST (1 to 1.5 V potential cycles) in MEAs. Two PtNiN samples on corrosion-resistant graphene were synthesized at Brookhaven National Laboratory by the third method using IUPUI-prepared Pt-seeded functional graphene (f-g) and nano-graphene (f-nanoG). Both samples met the support AST target at 0.9 V with <40% loss of Pt mass activity (Table 1). The voltage loss at high current densities (Figure 2a) was much less than that of Pt/HSC (Figure 2b) but needs to be further reduced to meet the support AST target at 0.8 A cm^{-2} (Table 1). Significant improvement in performance on graphene supports is expected by optimizing PtNiN synthesis on f-nanoG and more importantly by optimizing MEA fabrication. The catalyst layer forms a 3D architecture with spacers to keep graphene sheets apart. Functional groups on graphene, the size of spacer, and the solvent used during fabrication affect the porous channels formed. While adjusting these parameters takes time, the tunability offers opportunity for very best mass transport via optimal porosity and hydrophobicity.

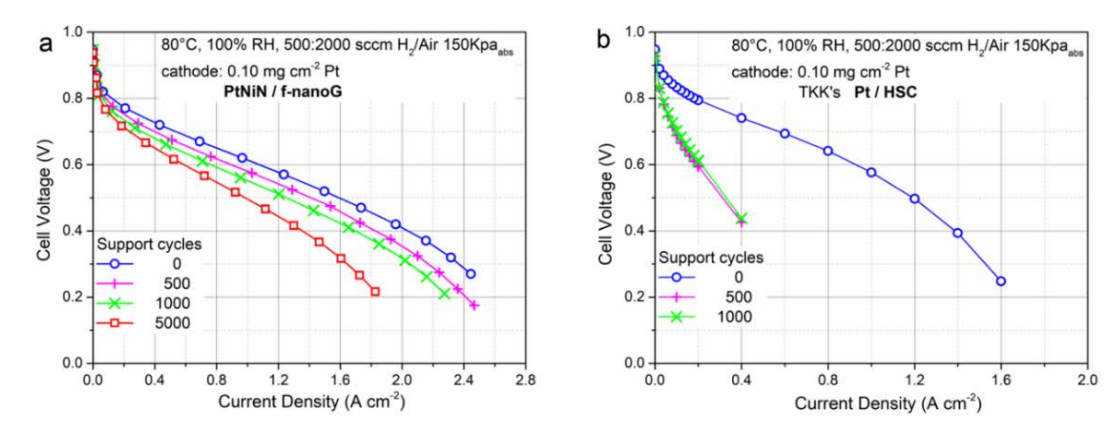

Figure 2. MEA polarization curves measured at IUPUI for testing support durability: (a) PtNiN on functional nano-graphene (f-nanoG), (b) Pt on high surface carbon (HSC) as a reference

In summary of MEA test results, four PtNiN samples tested by catalyst or support AST all showed limited activity loss at 0.9 V (<40%, exceeding the DOE target), which validates the effectiveness of nitriding in stabilizing Ni. Structural characterization carried out in FY 2019 clarified the X-ray diffraction (XRD) feature for crystalline Pt_{ML}-Pt_2Ni_2N nanoparticles and shed light on why PtNiN nanoparticles can be better than PtNi and comparable to $L1_0$ PtCo nanoparticles for ORR.

A Pt monolayer on a Pt-Ni-N core (Figure 3a) does not have enough contrast to be observable by scanning transmission electron microscopy with energy-dispersive X-ray spectroscopy (STEM-EDS). Its existence is deduced by the fact that Pt:Ni atomic ratio measured by EDS for whole particles is higher than the 1:1 Pt:Ni ratio suggested for the core region based on XRD-determined lattice strains. Figure 3b shows no apparent change in particle size, morphology, and element distribution after 30,000 catalyst AST cycles on rotating disk electrode in 0.1 M $HClO_4$. As can be seen from the high-angle annular dark-field (HAADF) image in Figure 3c, the Pt_{ML}-Pt_2Ni_2N particles remained solid-like and uniform. These features support that Ni is stabilized significantly by nitriding. In optimizing synthesis for Pt monolayer skin, symmetric diffraction peaks in XRD intensity profiles is the criterion for Pt multilayer skin being avoided because shoulders or asymmetric peaks emerge when the lattice spacing of Pt multilayer changes toward that of bulk Pt from that of PtNi nitride cores. If Ni loss after AST at 80°C in MEA needs to be further reduced, segregation of Pt during nitriding may be tuned for Pt bilayer formation.

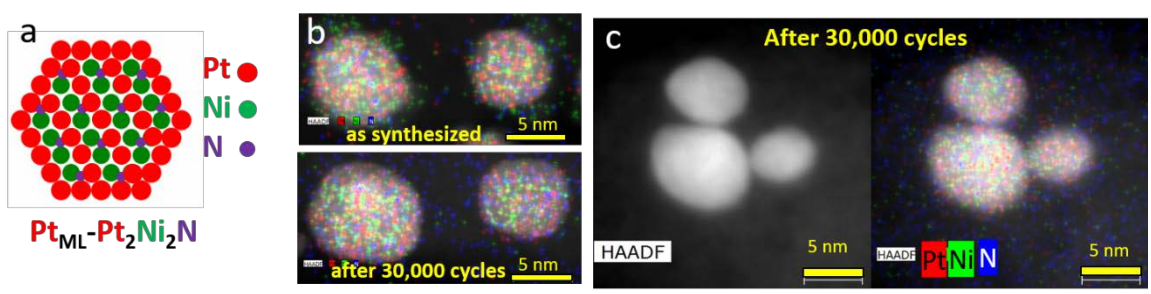

Figure 3. (a) 2D schematic model of a Pt monolayer on Ni-enriched bimetallic nitride core; (b,c) HAADF and EDS mapping of Pt_{ML}-Pt_2Ni_2N particles on VC

For bimetallic PtCo and PtNi nanoparticles with or without nitriding, lattice strain with respect to Pt is a key tunable structural parameter in enhancing specific activity for ORR. Figure 4 shows that Pt_2Ni_2N forms face-centered-tetragonal (fct) lattice and has similar strains as measured for fct-Pt_1Co_1, which is often called $L1_0$-Pt_1Co_1. The N atom is at the center of the unit cell as in the face-centered-cubic (fcc) Ni_4N lattice. For Pt_2Ni_2N, chemical ordering with Ni atoms preferably at the face-center sites causes larger contraction along one axis than the other two, which transfers the unit cell from cubic to tetragonal (i.e., from fcc to fct). Since powder

diffraction files for Pt_2Ni_2N are not available, those for Pt_1Co_1 and Pt_1Ni_1 are shown respectively in Figure 4a and 4b to illustrate that fct lattice can be distinguished from fcc by the strain measured at (111) and (200) diffractions being different (i.e., the symmetry factor, S(200)/S(111) <1.0).

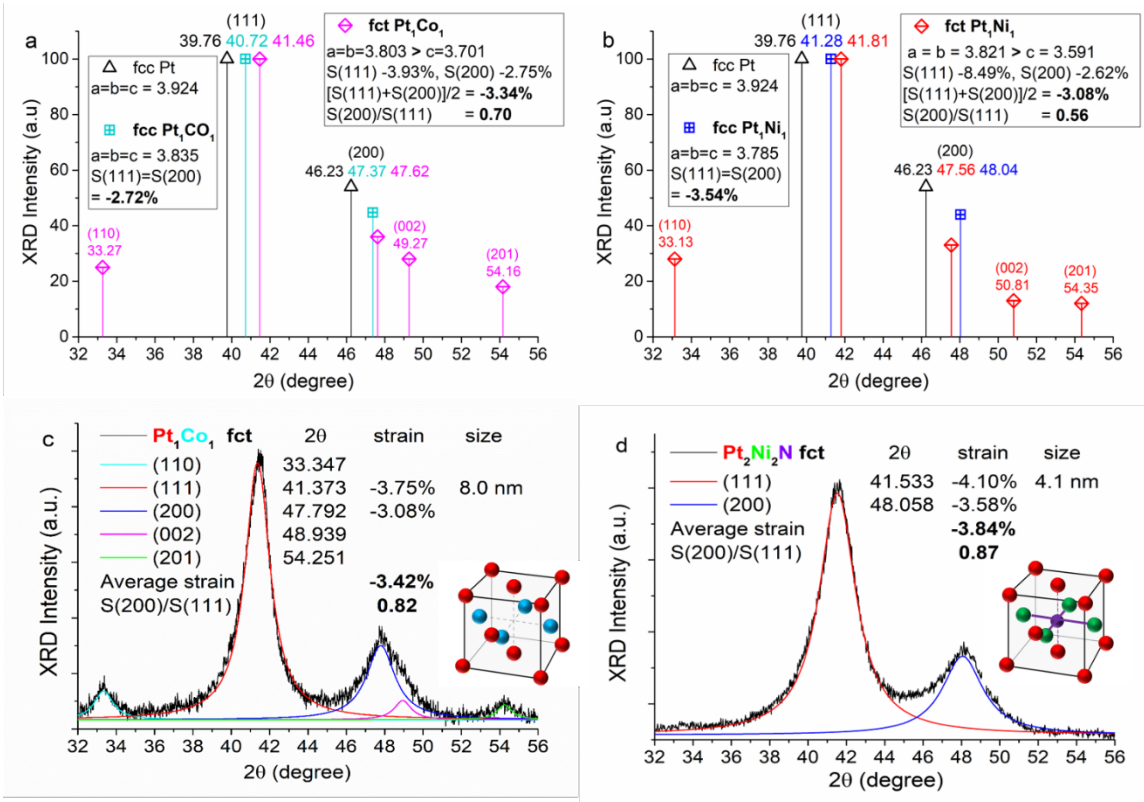

Figure 4. (a,b) XRD patterns for fcc and fct lattices of Pt_1Co_1 and Pt_1Ni_1 with fcc Pt as reference. Powder diffraction file numbers: Pt-fcc 03-065-2868, fcc-PtCo 03-065-8968, fct-PtCo 00-043-1358, fcc-PtNi 03-065-9445, and fct-PtNi 03-065-9446. (c,d) XRD profiles for a Pt_1Co_1/VC and a Pt_{ML}-$PtNi_2Ni_2N$/VC samples. Inserts show fct unit cells of Pt_1Co_1 and Pt_2Ni_2N (red dot for Pt, blue for Co, green for Ni, and purple for N).

Figures 4c and 4d show typical XRD profiles for fct-Pt_1Co_1 and fct-Pt_2Ni_2N nanoparticles with the symmetry factor being 0.82 and 0.87, respectively. The average strain, [S(111) + S(200)]/2, is comparable for fct-Pt_2Ni_2N (-3.84%) and fct-Pt_1Co_1 (-3.40%), showing larger lattice contractions than those calculated for the fcc-Pt_1Ni_1 (-3.54%) and for the fcc-Pt_1Co_1 (-2.72), respectively. Thus, formation of chemically-ordered fct lattices enhance not only structural stability but also ORR specific activity for PtNiN and PtCo. In contrast, as showed in Figure 4b, the average lattice contraction of fct-Pt_1Ni_1 (-3.08%) is smaller than that of fct-Pt_1Ni_1 (-3.54%). Thus, nitriding PtNi benefits not only durability but also the specific activity of nanocrystalline particles for ORR.

FY 2019 PUBLICATIONS/PRESENTATIONS

1. Z. Liang, L. Song, S. Deng, Y. Zhu, E. Stavitski, R.R. Adzic, J. Chen, and J.X. Wang, "Direct 12-Electron Oxidation of Ethanol on a Ternary Au(core)-PtIr(shell) Electrocatalyst," *J. Am. Chem. Soc.* 141 (2019): 9629-9636.

2. K. Sasaki, N. Marinkovic, and R.R. Adzic, "In Situ X-ray Absorption Spectroscopic Studies of Nanostructured Electrocatalysts for Fuel Cells," Di-Jing Huang, Li-Chyong Chen (eds.), World Scientific Publishing Co. (Taipei), in print.

3. K. Sasaki, "Electrochemical cells for in situ XAS studies," *International Tables for Crystallography: Volume I, X-ray Absorption Spectroscopy and Related Techniques*, C. T. Chantler, B. Bunker, F. Boscherini (eds), International Union of Crystallography (Chester, UK), in print.

4. Jia X. Wang, "Challenges and Opportunities in Developing Anode Catalysts for Direct Ethanol and Ammonia Fuel Cells," Electrochemical Society Meeting, Dallas, TX, May 28, 2019.
5. K. Sasaki, K.A. Kuttiyiel, and G.-G. Park, "Designing High Performance Low-PGM Electrocatalysts for Fuel Cells," Global Day Symposium, KIER, Daejeon, Korea, August 24, 2019.
6. C. Bell, D.C. Lee, K. Sasaki, and M. Williams, "A Versatile Architecture for Electronically Tunable Electrocatalytic Activity: Graphene-Templated Atomically Thin Pt Supported on Oxygen-Deficient Titania," 235th ECS Meeting, Dallas, TX, May 29, 2019.